Title Cutting-edge nanomaterials for advanced multimodal bioimaging applications

Author(s), and Corresponding Author(s): *Ming-Kiu Tsang, Yuen-Ting Wong and Jianhua Hao**

Ming-Kiu Tsang, Yuen-Ting Wong and Jianhua Hao*

Department of Applied Physics, the Hong Kong Polytechnic University, Hung Hom, Hong Kong, P. R. China.

* E-mail: jh.hao@polyu.edu.hk

Keywords: multi-modal bioimaging, upconversion, two-dimensional materials, gold, carbon, nanobubbles

Abstract: The desire for high sensitivity, resolution, low toxicity and fast clearance contrast agents has driven the research for new nanomaterial systems. The drawbacks of traditional molecular probes limit their bioimaging ability, hence the exploration of emerging nanomaterials for multimodal bioimaging continues with rational designs. The key for realizing effective multimodal bioimaging is harnessing the physical and chemical properties of the nanomaterials. Although some nanomaterials possess multimodality intrinsically, those imaging modes might not be sufficient to meet the increasing demand of various applications. Therefore, the fabrication of novel composite structures by integrating various nanomaterials or molecules may overcome the challenging issues in multimodal bioimaging. This review presents the overview and considerations for multimodal bioimaging and the requirements on

the nanomaterials. The recently emerged nanomaterials and their composite structures for multimodal bioimaging are highlighted, including the recent emerging two-dimensional materials. The traditional nanomaterials also showed breakthroughs in terms of novel structures and morphologies, in which would affect the contrast ability, entrance and clearance from the *in-vivo* models. Finally, some suggestions for toxicity studies of nanomaterials and new strategies are presented for realizing the advance of multimodal bioimaging.

1. Introduction

The visualization of internal organs and body structures has aided the understanding of different biological processes, the functions of organs and tumor diagnostics. The main obstacle of bioimaging is the physical properties of the levels of organization in organisms, such as the near-infrared (NIR) absorption by fat tissues[1], different X-ray absorption coefficients of soft/hard tissues[2] and the imaging depths or area of interest in the organs. These considerations drive the rapid development of imaging modes to reveal the desired information by different stimuli, such as light, magnetic field and ultrasound. Some body features of animals are able to provide contrast without any injections of contrast agents, for example, the red blood cells of animals are capable of reflecting ultrasound[3] while their bones may absorb X-ray.[4] However, the contrast agents are essential in some circumstances to enhance the contrast of structures or fluids for delicate images. Traditional imaging techniques have played important roles in biomedical imaging due to their superior imaging depths, such as computed tomography (CT), magnetic resonance imaging (MRI), positron emission tomography (PET) and single photon emission computed tomography (SPECT).[4] These imaging modes usually require contrast agents, generally known as functional organic molecules, including barium or iodine and radioactive tracers, which are used for CT and PET, respectively. However, these molecular probes show their respective limitations in

bioimaging applications, such as insufficient circulation time of iodine/barium-based molecules,[5] short half-life of radioactive fluorine-18 (^{18}F)[6] and high toxicity of the leaky gadolinium (Gd^{3+}) ions in Gd-chelates.[7]

These limitations offer new opportunities for nanoprobes to show their bioimaging abilities, taking advantages of their facile bio-functionalization and the enhanced permeability and retention (EPR) effect. Moreover, the size of the bottom-up synthesized nanoprobes could be tuned from around sub-ten to hundreds of nanometers by modifying the synthesis conditions.

In the family of nanoprobes, optical nanoprobes are unique in their emission properties because the engineered emissions can be used for fluorescent imaging (FI) or luminescent imaging (LI). The doped ions inside the host materials might also possess magnetism or X-ray absorption property. In the early stage of development, photoluminescent (PL) CdSe semiconductor quantum dots (QDs) had been exploited as the nanoprobe for bioimaging.[8] The high quantum yield and single excitation for multi-color emission had drawn substantial attention in the biomedical imaging field. Despite the excellent optical property, the high toxicity and PL intermittency (blinking)[9] limited their imaging ability. The toxicity was originated from the release of Cd^{2+} ions by photo-oxidation under ultraviolet excitation (UV).[10] Although the toxicity was reduced by shell coating, the shallow penetration of UV (around tens of micrometers[11]) was not favorable for *in-vivo* FI.

On the other hand, it should be noted that the nanoprobes are not necessary to be emissive, for instance, the commercialized microbubbles (MBs) typically with a size of 1-10 μm are good candidates for ultrasound imaging (USI).[12-14] They consist of a biocompatible shell of lipid, polymer or protein encapsulating a core filled with perfluorocarbon gas or air, which contributes to the large enchogenity difference for better ultrasound (US) contrast. In addition, MBs can even be modified with different shell materials for photoacoustic imaging (PAI).[15,16] Although they are readily commercialized, the probes are not able to reach the tumor site for USI diagnostics owing to the small pores (around 380-780 nm) of the blood vessels at tumor

site.[17] To date, extensive attempts on reviewing multimodal bioimaging applications by different nanomaterials were available in the literature.[18-24] Some of these reviews focused on single material system and the scope might be too broad. Therefore, we aim to provide a systematic and concise summary on the recent multimodal bioimaging development of these scattered groups of nanomaterials apart from some organic-based probes, such as the aggregation-induced emission luminogens[25] and metal-organic framework.[26] In particular, nanobubbles and two-dimensional (2D) materials including their derivatives are seldom reviewed. To start with, the common imaging modes and their respective features are summarized and discussed. Then, the overview of the spectrum of some nanomaterials for multimodal bioimaging including gold nanostructures, carbon quantum dots (CQDs), lanthanide (Ln^{3+}) ions-doped upconversion nanoparticles (UCNPs), echogenic nanobubbles (NBs) and 2D materials along with their derivatives is presented. Subsequently, the recent advances of different classes of nanomaterials and their conjugates for multimodal bioimaging are reviewed with typical examples. Finally, we present emerging candidates for multimodal bioimaging and suggestions on the future development.

2. Overview of multimodal bioimaging and nanomaterials

2.1. Multimodal bioimaging

The common imaging modes and instrumentations are listed in **Table 1**. These imaging modes possess their respective features, advantages and limitations. The rationale of developing multimodal imaging is to understand the strength and weaknesses of each imaging mode, and combine different modes in a single material system for synergetic imaging. The typical example is the combination of PET/CT[27], which allows the radiologist to obtain superior structural information and functional information of organs. In addition to PET/CT,

the integration of MRI/SPECT/FI not only enable the visualization of the interested tissues and biodistribution of the imaging probe but also the quantification of the probe *ex-vivo* using fluorescence (FL).[28] Importantly, the FL absorption and emission properties of the nanoprobes can be tailored to fit the biological windows (around 700-900 nm[29] and 1000-1700 nm[30]) for improved penetration and resolution in the *in-vivo* multimodal images, such as the imaging of mouse brain at a depth of more than 2 mm.[31] Moreover, the trimodal upconversion luminescence (UCL)/MRI/CT bioimaging[32,33] allows deep tissue imaging via the selection of MRI/CT imaging modes towards targeting organs while UCL imaging was known to be sensitive and displayed superior planar resolution. The above examples have showed the strategic choices of modalities for multimodal bioimaging.

Table 1. Summary of imaging modes

Imaging mode	Selected imaging system	Strengths	Weaknesses	References
FI/LI	*In-Vivo* FX PRO (Bruker)	• Good planar resolution (~100 nm) • High sensitivity	• Shallow imaging depth (~ 2 mm) • No 3D information	• 31, 34, 35
MRI	SIGNA (GE Medical Systems)	• Non-ionizing • Soft tissue imaging	• Not suitable for patient with metallic implant • Noisy	• 36

CT	Discovery CT750HD (GE Healthcare)	• 3D information available • Relatively cheaper	• Ionizing radiation • Low sensitivity	• 37
PET	Inveon (Siemens)	• Functional information of organs available	• Low spatial resolution (~1-2 mm) • Shorter half-life of tracers (110 min for ^{18}F)	• 38, 39
SPECT	NanoSPECT/CT (Bioscan)	• Cheaper than PET • Longer half-life of tracers (up to tens of hours)	• Low spatial resolution (~ 1-2 mm) • Long scan time	• 39, 40
USI	Vevo LAZR (Fujifilm)	• Non invasive • Portable	• Limited field of view • Obstructed by bones	• 41
PAI	Vevo LAZR (Fujifilm)	• High spatial resolution 100-400 µm	• Costly pulse laser • Disturbed by	• 42, 43

	resolution at the depth of several centimeters) • Low acoustic scattering	acoustic absorbing object

2.2. Nanomaterials

Apart from the imaging modes, it is worthwhile to exploit the properties of the cutting-edge nanomaterials for multimodal bioimaging. The types of nanomaterials for multimodal bioimaging are summarized in **Figure 1.** Owing to the rapid development of nanomaterials and conjugation techniques, the as-synthesized materials may have already demonstrated intrinsic multimodal bioimaging property. However, some of the material systems require surface modifications to immobilize the functional ligands or moieties for additional bioimaging modes. For example, the intrinsic magnetism of Gd^{3+} ions and iron oxide (Fe_3O_4) nanoparticles can readily support the MRI mode while the radioactive tracers, such as ^{18}F and copper-64 (^{64}Cu) isotopes, can emit gamma radiation for nuclear imaging modes. These functional materials form composite structure with the nanomaterials via doping, electrostatic attraction, covalent coupling, and so on. Interested readers may refer to other reviews for more knowledge on surface modifications and composite formation strategies.[44-47] Gold materials possess unique plasmonic absorption property as their size shrinkage to nanoscale. By converting photons into phonons, conventional gold nanoparticles (AuNPs) or nanorods (AuNRs) can induce remarkable photothermal effect and this is not only useful for thermal therapy and acting as optical quenchers[48] but also PAI. The atomic mass of gold is also relatively large to absorb X-ray for contrast in imaging. Since the gold nanostructures exhibit

irreversible aggregation in aggressive medium, one of their key features is the need for passivation, commonly with the use of polyethylene glycol ligands or functional shells. Moreover, the rapid renal clearance of the gold nanomaterials was validated in the literature.[49-51] As a result, these aspects manifest the basis for multimodal bioimaging. On the other hand, carbon is a light and abundant material with low toxicity to organisms[52-54], it is advantageous to harness the synthetic conditions and the physical properties for biodiagnoistic applications. It is crucial to distinguish the differences between carbon nanodots (CNDs) and CQDs to avoid confusion in terminology. In general, CNDs and CQDs can be distinguished from their crystalline structures and the hybridization state of the carbon atoms in these structures.[55,56] Nevertheless, CNDs and CQDs are both PL materials; except that the origin of the luminescent mechanism can be additionally attributed to surface detects or zigzag edges other than the well-known quantum confinement. Similar to gold nanostructures, carbon nanostructures with remarkable photothermal effect are an effective PAI contrast agent. In contrast to the traditional PL nanomaterials, UCNPs offer non-invasive and tissue penetrating NIR excitation for UCL. It is well-known that NIR radiation is optically transparent to biological tissue and hence exhibiting higher penetration depths for *in-vivo* applications. Conventional fluorescent materials, such as organic dyes and QDs are usually excited by UV or visible light[57] while the wavelengths for UCL are employed at 980 and 808 nm due to the doping of Yb^{3+} and Nd^{3+} ions, respectively.[58] Notably, sensitization of UCNPs at 808 nm is superior to that at 980 nm because of minimized water absorption for better tissue penetration.[29] However, the mechanism for 808 nm-harvested UCL is different to that of 980 nm because of the need for core-shell structure.[59,60] The optical energy can be transferred from core to shell region via the spatially separated Ln^{3+} dopants without severe cross relaxations. In addition to the excitation wavelengths, the Ln^{3+} ions in the UCNPs also offer surpassing physiochemical properties including long lifetime, large anti-Stokes shift, narrow and sharp emission peaks (10-20 nm full width half maximum)[61], absence of

autofluorescence, low toxicity, high resistance against photoblinking (up to 3 hours)[62] and bleaching. Therefore, UCNPs had been widely used in nano-biosensing and bioimaging works.[63,64] The high atomic mass of Ln^{3+} ions and special electronic configuration of Gd^{3+} ions enable the UCNPs with magnetism and X-ray absorption ability, hence UCNPs are commonly used as nanoprobes for multimodal bioimaging.[65,66] In addition to optical probes, the similar enchogenity of organ tissues and blood vessels manifests the demand for advanced ultrasound-enhanced contrast agents (UCAs) to generate contrast of large tissues, especially tumor sites. Therefore, more light has been shined onto novel NBs with a size less than 1000 nm for effective extravascular multimodal imaging.[67] The shrinkage from MBs to NBs endows the NBs with typical EPR effect of nanoprobes. The intrinsic NBs show enchogenity for single USI mode or USI/PAI mode depending on shell materials, they might need further surface conjugations of functional molecules for multimodality. 2D materials are few-layer atomic thick, therefore their electrical transportation and optical properties had attracted a substantial amount of attention in the optoelectronic and electronic device field.[68-72] Graphene and graphitic carbon nitride are typical examples of 2D materials that had been extensively studied in the previous researches,[73-76] whereas the 2D transition metal dichalcogenides (TMDs), hexagonal boron nitride (h-BN) and black phosphorous (BP) nanosheets emerged as a new class for biological applications, the cytotoxicity studies indicated that they were biocompatible.[77-79] Moreover, previous reports even showed that TMDs might enhance cell uptake due to improved ligand-receptor interaction.[80,81] The NIR absorption and heavy metal atoms in 2D TMDs provide intrinsic PA/X-ray contrast while the 2D QDs prepared from their 2D parents possess FL property due to quantum confinement and edge effects.[82] These attractive properties enable the 2D materials and their derivatives as a potential platform for multimodal bioimaging.

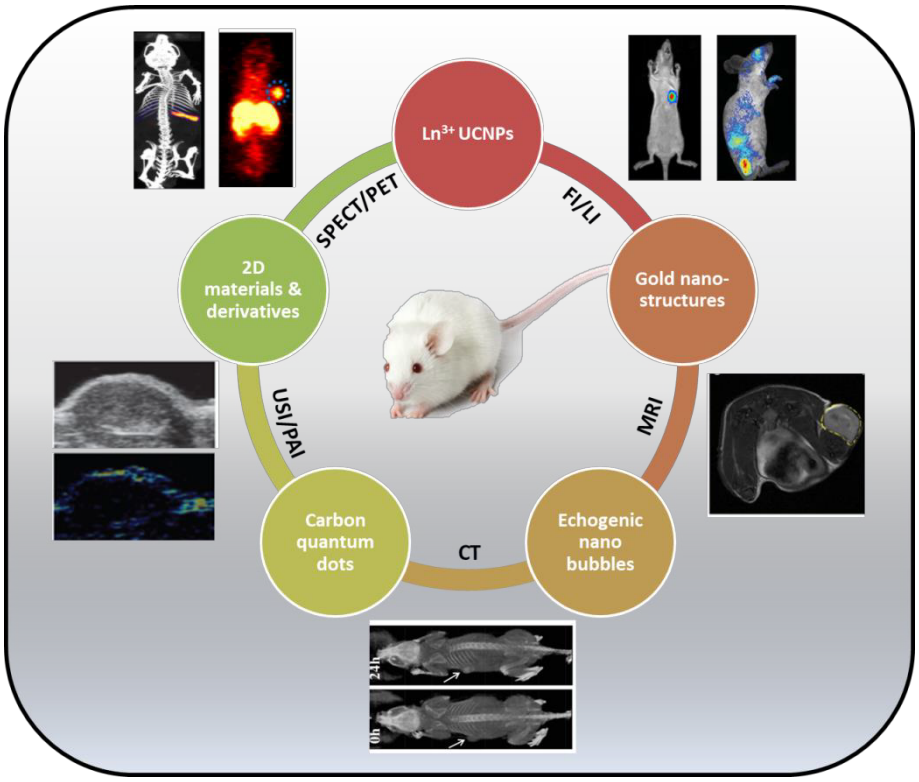

Figure 1. Summary of cutting-edge nanomaterials for multimodal bioimaging.

3. Cutting-edge nanomaterials for multimodal bioimaging

3.1. Gold nanostructures

The structural engineering of gold nanostructure enabled the preparation of different morphologies, such as nanoprism[83], nanostar[84], nanocage[85], nanoshell[86] and nanotripods.[87] They are basically formed from nucleation, followed by directional growth in the presence of surfactants. Therefore, the plasmonic property of the yielded structures can be modulated by different shapes. Su and co-workers prepared a yolk-shell structure of AuNRs with porous Fe_3O_4 shell for MRI/PAI image-guided drug therapy.[88] The reported technique differs from the conventional direct conjugations because of the non-contact nature between AuNRs and Fe_3O_4. This avoided the undesired limited attaching, inferior magnetic property and plasmonic peak broadening. The dual-modal MRI/PAI monitored the drug release profile in a real time manner. In another report, Kohane and co-workers synthesized gold nanostars

(AuNSs) capped with metal-drug polymer shell for image-monitored therapy.[89] The use of nanostar structure increased the surface area for drug loading. In addition to MRI, the two-photon luminescence could be used for monitoring the distribution of the AuNS in the 4T1 tumor at microscopic level. The effort to tune and synthesize anisotropic gold nanoarchitectures for enhanced plasmonic property can be beneficial to bioimaging because of improved contrast ability and clearance. Cheng et al. presented their systematic validation of forming gold nanotripods (AuNTs) for multimodal bioimaging.[87] The proof of the tripod structures (tripod-T and tripod-A) (**Figure 2**(a)) was accompanied with stringent synthetic conditions and numerical simulation analysis of the electric field intensities at different planes. After that, the AuNTs were functionalized with RGDfc peptide and ^{64}Cu for targeted dual-modal PAI/PET bioimaging. The biodistribution of the functionalized AuNTs was studied by using PET scans, revealing that the functionalized AuNTs were almost cleared via hepatic and renal excretion. Moreover, the tumor uptake was supported by using blocking dose of c(RGDfc), attributed to the targeting function of the peptide. Apart from PET, the PA intensities yielded a linear relationship with the concentrations of the injected AuNTs. It was found that the functionalized AuNTs at the tumor site were around 200 pM. In addition to the relatively bulky structure, the size of gold can even be shrunk down towards molecular scale as gold nanoclusters (AuNCs)[90], showing fluorescence and even additional ferromagnetism.[91] A new strategy for the bio-synthesis of AuNCs-Fe complexes in tumors was discovered by using $[AuCl_4]^-$ and Fe^{2+} ions as precursors.[92] The preliminary FI results fostered further investigations on the formation of the AuNCs-Fe complexes from the tumor extract. Subsequently, MRI and CT were performed in HepG2 xenograft tumor mice to examine the multimodality of the AuNCs-Fe complexes. In addition, the mice were sacrificed and the internal organs were examined by FI to evident the biodistribution and biocompatibility (Figure 2b). The novel *in-situ* route might enable possibility of clinical diagnosis of deeply seated early neoplasms. The combination of AuNPs and AuNCs to form

quantum rattles (QRs) in a hollow mesoporous silica shell can maximize the performance of gold nanostructures for multimodal bioimaging.[93] The AuNCs featured paramagnetism, NIR fluorescence and photothermal properties while the immobilized AuNPs in the hollow cavity provided a hydrophobic zone to load the doxorubicin (DOX) for drug delivery. The multimodality property was further evaluated in a murine colorectal carcinoma tumor model after justifying the entrance pathway of the QRs in cell model. Figure 2(c)-(f) depict the multimodal *in-vivo* imaging of the QRs in LS174T-luc tumor model in CD1 nu/nu mice. The NIR FI result suggested the accumulation of the QRs at the tumor site with the support from the control experiment using bare hollow mesoporous silica shell (Figure 2(c)). Furthermore, Figure 2(d) clearly shows the enhanced MRI of the tumor, indicating the distribution of the QRs at the tumor site. Additionally, the PAI was performed by using 670 nm laser as presented in Figure 2(e) and (f). The PA signal from the QRs was processed with false yellow color; the QRs exhibited enhanced PA contrast despite the strong PA signal from the blood vessels.

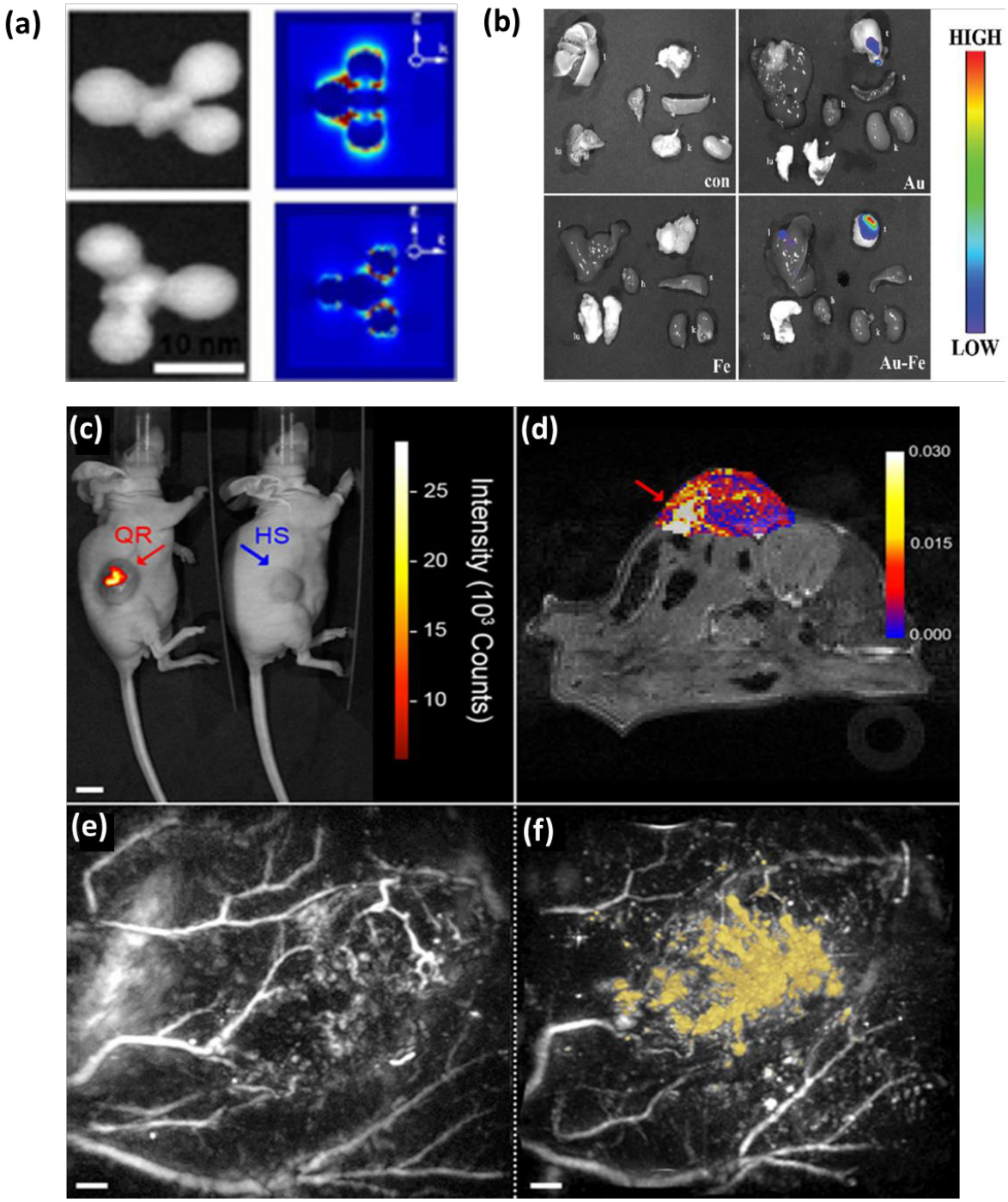

Figure 2. (a) Scanning transmission electron microscopy image and the numerical simulation analysis of the two types of AuNT (The upper panel shows the image and yz plane electric field intensity at 700 nm of tripod-T while the lower panel is tripod-A),[87] (b) *Ex-vivo* FL examination of major organs (l for liver, t for tumor, h for heart, s for spleen, lu for lump, and k for kidney) from U87 xenograft mice models in different groups (control (con), Au, Fe, and Au-Fe) at 48 h post injection,[92] (c) NIR FI of the QRs and bare hollow mesoporous silica

shell (HS) in the LS174T-luc tumor model in CD1 nu/nu mice, (d) MRI of the tumor showing the longitudinal relaxation rate, the red arrow indicates the focal point of increased relaxation rate. The PAI (e) before and (f) after irradiated by 670 nm laser. The false yellow color represented the PA contrast by the QRs, the scale bar is 1 mm.[93]

3.2. Carbon quantum dots

Carbon nanotubes are traditionally regarded as promising materials for PAI owing to their ability to produce ultrasound waves upon pulsed laser excitation.[94-99] In addition, recent reports indicated that Gd^{3+} ions were successfully doped into the carbon host matrix to endow magnetism to the material.[100-102] Therefore, the multimodality performance of the carbon-based quantum dots can be validated in cell or small animal models. One of the early works regarding the use of CQDs for *in-vivo* FI was done by Sun and co-workers.[103] The CQDs were injected via different pathways and the FI studies provided evidence for the biocompatibility of CQDs for future *in-vivo* applications. In a later work, they prepared brain cancer-targeting CQDs by simple pyrolysis route.[104] Importantly, the FI results indicated the blood-brain-barrier penetration ability of CQDs. This work showed the high potential of CQDs as smart nanomedicine. Recently, Su et al. reported the dual-modal FI/MRI by using CQDs-decorated Fe_3O_4-silica core-shell nanocomposite.[105] The nanocomposite was functionalized with folic acid to accomplish target imaging and the results suggested high cell uptake of the nanocomposite. By using a similar approach, Liu et al. stabilized Fe_3O_4 with nitrogen-doped CQDs for trimodal FL/MRI/CT *in-vivo*.[106] The multifunctional structure exhibited high FL quantum yield at around 21 % with small average size of 11 nm. The tumor in the mice was clearly observed by FI, MRI and CT. In addition, the biodistribution study indicated the EPR effect of nanoprobes at tumor site. The injected Fe_3O_4-CQDs were mostly cleared via urine excretion pathway after two hours of injection. At this point, one should realize the biocompatibility of CQDs to living organisms and its flexibility for conjugating

with other nanomaterials for nanocomposites. Apart from conjugates, CQDs can be doped with different ions to strengthen their imaging performance. Yao et al. showed that Gd^{3+}, Eu^{3+} and Mn^{2+} ions could be doped into CQDs for dual modal FI/MRI.[107] The waste crab shell was used as the precursor for preparing the CQDs with different doping and a high survival rate of the embryonic development of zebrafish culture incubated with the doped CQDs suggested the good biocompatibility of the CQDs. On the other hand, red emissive CQDs are beneficial for bioimaging with their merits of the high tissue transparency in the range of 650-950 nm.[29] Ge et al. synthesized a type of CQDs using polythiophene phenylpropionic acid as precursor.[101] The as-prepared CQDs showed intense red emission at 640 nm and a photothermal conversion efficiency up to 38.5 %. These properties were highly suitable for FI and PAI. **Figure 3** presents the *in-vivo* and *ex-vivo* FI and PAI. It could be observed that the accumulation of the CQDs at the tumor site due to the EPR effect (Figure 3(a)). Figure 3(b) and (c) show the relative FL intensities of different internal organs in a sacrificed mouse and strong FL signal was detected in the tumor attributed to the CQDs uptaken. The highest FL intensity was observed at around 5 h post injection and dropped steadily until 24 h (Figure 3(d)). Moreover, Figure 3(e) presents the PAI at different time points after injection. The strongest PA signal was recorded at 6 h post injection, which was similar to the results in FI. The enhanced contrast indicated that the CQDs were a promising candidate for biodiagnoistic applications.

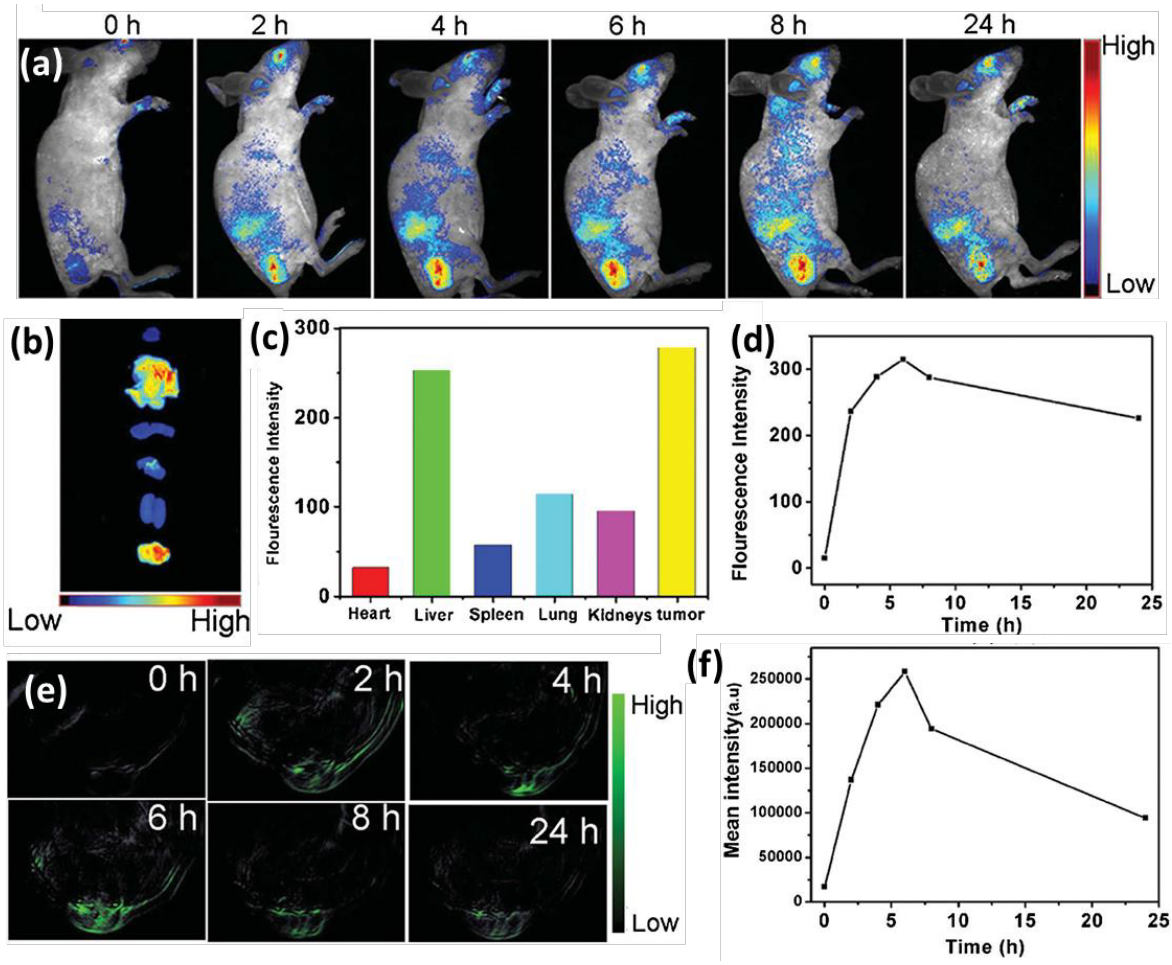

Figure 3. (a) Real-time *in-vivo* FI after injection at different time intervals, (b) *Ex-vivo* FI of the mice tissues (From top to bottom: hear, liver, spleen, lung, kidneys and tumor), (c) FL intensities of the mice tissues, (d) Average FL intensities at the tumor area over 24 h, (e) PAI of tumors in mice after injection of CQDs at different time intervals and (f) Mean PA intensities at the region of interest over 24 h.[108]

3.3. Ln^{3+} ions-doped upconversion nanoparticles

In recent years, UCL nanoprobes have been extensively introduced for diverse theranostic applications. For example, Han et al. proposed NIR-activated drug delivery systems using silica-coated $NaYF_4$:Yb/Tm UCNPs coupling with AuNPs.[109] However, the single UCL imaging modality responsible for therapy activation cannot effectively provides a real-time report of the UCNPs distribution in case any damages are posed to the intact cells. To overcome this limitation, multimodal nanoprobes are highly demanded to provide complementary data for the diagnosis. The T_1-weighted magnetic properties of Gd^{3+} ion-doped UCNPs are useful for MRI/UCL dual-modal imaging.[110-113] MRI modes of MR angiography (MRA) and MR perfusion (MRP) were firstly exploited in nontoxic PEGylated $NaYF_4$:Yb^{3+}/Er^{3+}@$NaGdF_4$ UCNPs.[114] Given by the negative-lattice shielding effect of Gd^{3+} ions, the core-shell UCNPs exhibited excellent T_1 relaxivity of 3.2 folds higher than the commercialized Magnevist® contrast agent, sophisticatedly giving high-resolution MRA image of the vascular system in rat models. For the sake of better tissue penetration, it is always desirable to integrate NIR-to-NIR UCL into the multimodal nanoprobes. By harvesting excitation in biological transparency window, neodymium (Nd^{3+}) dopants pose minimized heating effect for deeper UCL imaging of bio-tissues.[115] Li. et al. has prepared rose bengal (RB)-decorated $NaGdF_4$:Yb/Er@$NaGdF_4$:Yb/Nd UCNPs by thermal decomposition for efficient photo-controlled PDT of 4T1 breast cancer cells *in-vitro* and *in-vivo*.[116] The UCNPs exhibited not only NIR-to-NIR UCL but large r_2/r_1 relaxivity ratio of 75 at 7 T for ultra-high field T_2-weighted MRI, which were important to achieve real-time image-guided PDT without significant photothermal damages. Apart from the Ln^{3+} ion-based MRI contrast agents, UCNPs coated by paramagnetic Fe^{3+}-containing metal-organic framework (MOF) were examined as UCL/MRI dual-modal contrast agents.[117] The well-agreed MRI and UCL contrasts proved the success of targeted imaging of KB cells and KB

tumor-bearing mice by the folic acid-conjugated UCNP@MOF. Due to high penetration depth and good spatial resolution of PAI, a nanocomposite consisting of Nd^{3+}-doped multi-shell UCNPs and indocyanine green (ICG) dye has been established for trimodal UCL/PAI/MRI imaging.[118] Small blood vessels at a deep depth of 4.8-10 mm under the skin of SCC7 tumor-bearing mice were clearly imaged by the strong PA contrast from ICG. Radioactive tracers are responsible for PET and SPECT to acquire 3D structural images with the help of CT scan. Interestingly, Li's group integrated these two imaging modalities individually into UCNPs by using ^{18}F[119] and Samarium-153 (^{153}Sm)[120,121] to achieve UCL/PET (or SPECT). By detailed and systematic investigations, ^{18}F-decorated UCNPs were promising PET scan contrast agent while ^{153}Sm-containing UCNPs were a good blood pool agent with long circulating time. Recently, Rieffel et al. incubated ^{64}Cu radioisotope as PET tracers in porphyrin-phospholipid (PoP)-coated $NaYbF_4$:Tm@$NaYF_4$ UCNPs and six imaging modalities of UCL/FL/PAI/PET/CT/Cerenkov luminescence (CL) was demonstrated.[122] This may give a new insight for the development of hyper-integrated imaging systems. By assembling AuNR dimer with chlorine6 (Ce6)-labeled UCNPs, a novel core-satellite theranostic agent with UCL/PAI/CT/MRI capabilities was created for effective image-guided combined phototherapies (**Figure 4**(a)).[123] Images of the NR dimer-UCNP-Ce6 assemblies were obtained at 0, 4 and 24 h post-injection based on the multiple imaging techniques (Figure 4 (b)-(e)), in which much stronger contrasts were observed after 24 h post-injection. The results had justified the efficient passive-targeting ability of the assemblies and demonstrated the possible real-time image-guided therapies. By comparing to numerous control groups, NR dimer-UCNP-Ce6 assemblies performed excellent photothermal therapy to the HeLa tumor-bearing mice as indicated by a rapid temperature rise from 25.1 to 56.5 °C within 5 min of 980 nm laser irradiation. The combined therapies efficiency was also monitored by tumor size measurement over 15 days and the treatment with NR dimer-UCNP-Ce6 resulted in complete elimination of the tumor without any observable re-growth.

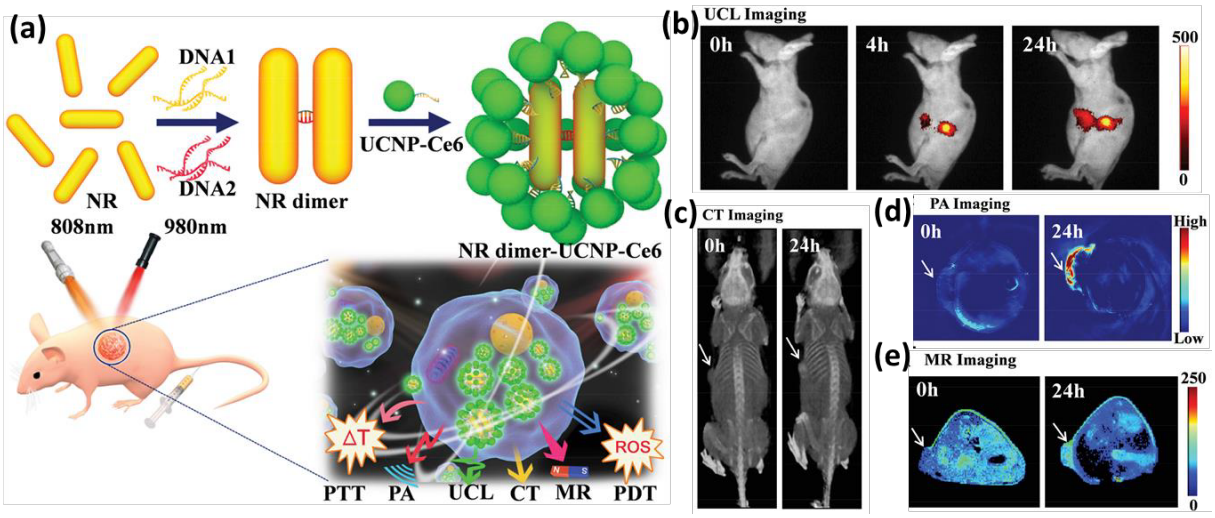

Figure 4. (a) Schematic illustration of DNA-based AuNR dimer and UCNP core-satellite assembly for multimodal imaging guided combination phototherapy. (b) UCL imaging, (c) CT, (d) PAI, and (e) T_1-weighted MRI of HeLa tumor-bearing mice taken at different time points after intravenous injection with NR dimer-UCNP-Ce6 (200 μL 2 mg mL^{-1}, in terms of the AuNR amount).[123]

3.4. Echogenic Nanobubbles

One of the motives for NB development is to overcome the size limitation of MBs to enter tumor sites. Huang and co-workers had investigated on the penetration ability of PEGylated lipid NBs to tumor site using gastric cancer xenograft as the studying model.[124] Their results indicated that the NBs were able to penetrate the endothelial cells of the tumor and entered the tissue space. In a similar report, the conjugation of NBs with fluorescent Affibody and HER2 antibody had validated the *in-vitro* and *in-vivo* USI ability of NBs.[125] The NBs-Affibody conjugates were also compared with the commercialized SonoVue® MBs in term of the size property. The NBs-Affibody conjugates were able to pass through the tumor capillaries and the MBs only accumulated at the tumor vessels. Song et al. demonstrated the trimodal MRI/USI/PAI *in-vitro* using Herceptin-decorated and superparamagnetic iron oxide nanoparticles/paclitaxel-embedded NBs (PTX-SPIONs-HER-NBs).[126] The fine structure was

fabricated by combining a modified double-emulsion evaporation process with carbodiimide technique. The preliminary studies from the cell model were expected to extend to *in-vivo* model. The concept of stimuli responsive nanomaterials[127,128] can also be applied in NB-based composite fabrications. Huang et al. fabricated NBs for dual modal MRI/USI bioimaging and US-triggered drug release by using thermo-responsive polymer.[129] The nanocomposite consisted of a perfluoropentane (PFP) core with SPIONs encapsulated in the Pluronic F127 polymer shell. The fabrication sequence shown in **Figure 5**(a)-(d) was performed in an emulsion consisting of the SPIONs, drug (BCNU) and dichloromethane solvent. The thermo-responsive polymer could form a stable hollow structure loading the hydrophobic Fe_3O_4 nanoparticles via the two-step annealing process and the core was then filled with the perfluoropentane gas. Moreover, Figure 5(e) shows US image of the glioma tumor of mice, which was marked with a yellow circle. Additional US contrast was observed in Figure 5(f) due to the application of magnetic targeting (MT). The corresponding MR images in Figure 5(g) and (h) agreed well with the contrast in the USI mode, attributed to the accumulation of SPIONs. On the other hand, it is worthy-noting that the trade-off among size, echogenic contrast enhancement and therapeutic efficiency of UCAs recently endowed the *in situ* size-converting UCAs desirable to achieve effective extravascular USI. For instance, Paproski et al. showed the transformations from porphyrin nanodroplets (NDs) to MBs by using high pressure US[42] and Liu et al. utilized the transformation of magnetic nanoliposomes to MBs inside the tumor cells to burst the tumor.[130] These examples suggested the high potential of the strategy for advanced imaging routes. Emelianov and co-workers presented their systematic study on using ICG-loaded perfluorocarbon (PFC) NDs for enhanced PAI and USI.[131] Although there was no biological species demonstration in the work, a polyacrylamide tissue-mimicking construct was used to prove the proof-of-concept transformation. The ICG molecules acted as the photosensitizer and the loading into the PFC NDs was confirmed by confocal microscopy. The basic principle of the droplet to NBs

transformation was the vaporization of the liquid in the droplet, therefore enhanced contrast-to-noise PA and US signals were observed upon the irradiation of pulse laser. Huynh et al. showed another transformation route from porphyrin MBs to NBs by using low frequency US pulses (conversion pulses).[132] The porphyrin MBs were transformed into NBs in the range of 5-500 nm and the pulse-dependent transformation was examined with the multimodal USI/PAI/FI signals. Stronger PAI/FI signals but weaker USI signals were obtained with an increased number of conversion pulses. The success of the size-conversion was also validated in the *in-vivo* multimodal bioimaging of KB-xenograft-bearing mice exposed to conversion pulses. Figure 5(i) shows a decrease in US contrast due to the conversion pulses applied after 20 s post injection and this also supported the circulation of the MBs to the tumor site. In consistent with the pulse-dependent study, enhanced PA contrast was clearly observed in the tumor xenograft irradiated by conversion pulses (Figure 5(j)), suggesting the *in-situ* transformation from MBs to NBs. It was also remarkable that the transformation contributed to better EPR effect of the material to give PA contrast lasting for at least 2 h, while the group without conversion pulse recorded a quick decay in PA contrast in 30 min. This work introduced a new opportunity for US-based transformation methods in multimodal bioimaging.

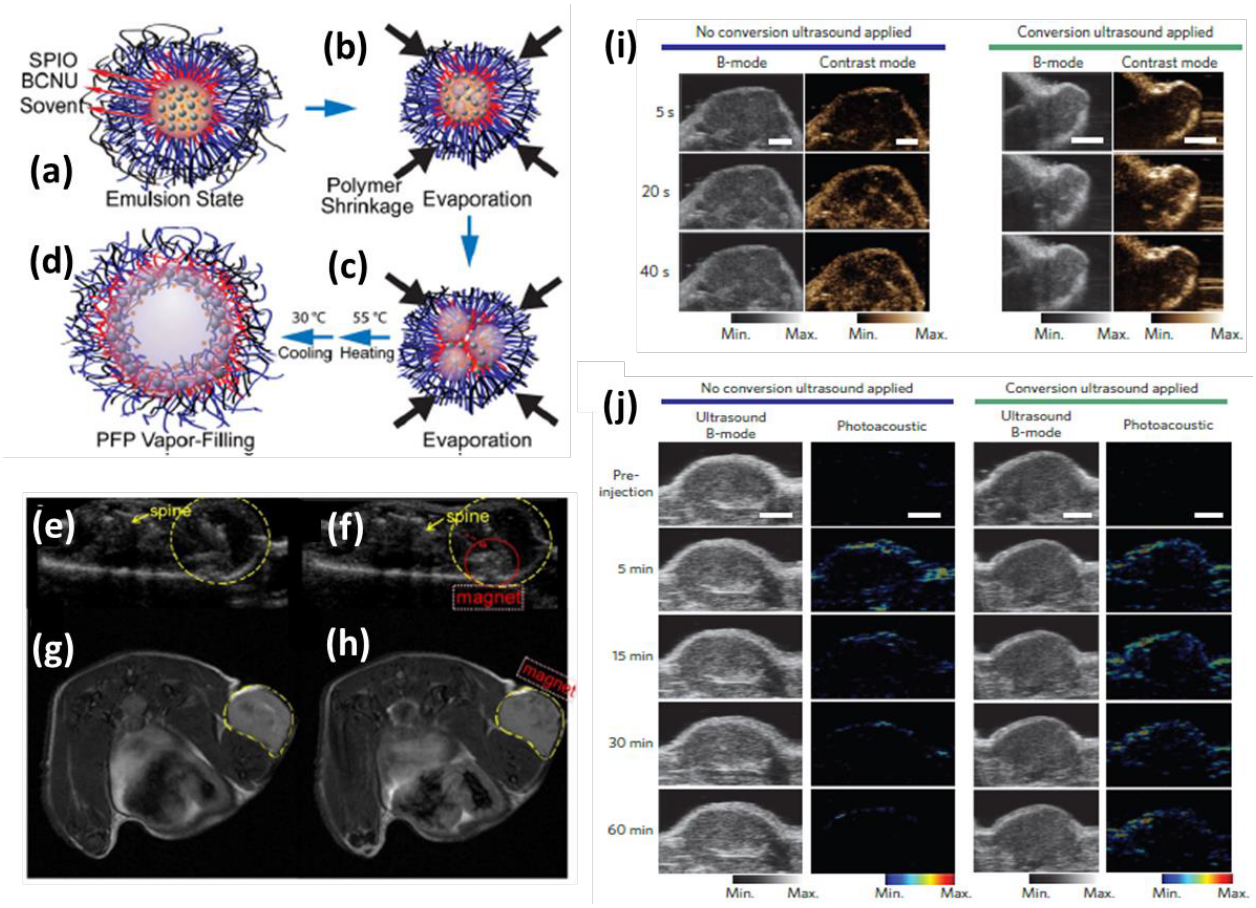

Figure 5. (a)-(d) Schematic mechanism and sequence for the fabrication of SPIONs encapsulated NBs in the emulsion consisting of SPIONs, BCNU and the solvent. USI of the glioma tumor of the mice (e) before MT and (f) after MT. The corresponding MRI of the tumor (g) before MT and (h) after MT. The darkening indicated the accumulation of SPIONs and yellow marking was the tumor site.[129] (i) Porphyrin MBs were intravenously injected into KB xenograft-bearing mice and a cross-section of the tumor was imaged using high-frequency US. Left: The MBs circulated into the tumor without conversion pulse (Scale bars, 2 mm). Right: Conversion pulse was applied after the 20 s time point, a decrease in contrast mode US signal was observed, for example at 40 s. (Scale bars, 3 mm). (j) Conversion of porphyrin MBs to NBs in tumor xenografts enabled the retention of NBs in the tumor, as confirmed by PAI. PA images of the tumor xenograft are shown without or with conversion pulse applied at pre-injection and 5 to 60 min. (Scale bars, 2 mm).[132]

3.5. Two-dimensional materials and their derivatives

2D materials are single or few layered-structure materials, in which the inter-layers are held by weak van der Waals' forces while the atoms in the 2D plane is connected by strong ionic or covalent bonds.[133] The first report about the doping of erbium (Er^{3+}) ions into 2D MoS_2 was achieved by using a modified chemical vapor deposition,[134] in which presented NIR-NIR UCL and downshifting luminescence (DSL) properties. The Er atoms were identified by using STEM as indicated in **Figure 6**(a). The atomic contrast of Er differentiated them from the Mo and S atoms. The emission spectra of Er-doped MoS_2 are shown in Figure 6(b) and (c), in which single 980 nm laser can simultaneously realize NIR-NIR UCL and DSL. These wavelengths may be useful for bioimaging owing to the high transparencies at the NIR I and NIR II windows. Apart from optical properties, transition metal dichalcogenides (TMDs) are mostly studied group among the family of 2D materials for multimodal bioimaging, because of their relatively heavy atomic mass for potential X-ray contrast. Moreover, their NIR absorption can also support PAI. Therefore, the dual modal CT/PAI had been explored in the 2D TMDs. Liu and co-workers synthesized PEGylated WS_2 nanosheets for CT/PAI-guided photothermal therapy.[37] The WS_2 nanosheets were prepared by breaking the interlayers of bulk WS_2 using Li^+ ions and sonication. The CT images suggested the PEG-WS_2 nanosheets were effectively uptaken by the 4T1 tumor-bearing mice via the reticuloendothelial systems. Moreover, the PAI experiment revealed that intravenous injection resulted in more uniform signal distribution throughout the whole tumor structure. Wang et al. utilized a one-pot solvothermal method to synthesize MoS_2/Bi_2S_3 composite with PEG passivation.[135] The reported synthetic route overcame the concerns of toxic gaseous byproducts released from the conventional technique. It was found that the CT imaging ability of the composite was enhanced in comparison to that with the same Bi concentration and their superior CT ability was regardless of injection methods. Despite the increase in PA signal, the CT/PAI abilities of the composite can be improved with targeting functions. By the integration with magnetic

species, the modality of TMDs can be extended to MRI. Yu et al. fabricated a MoS_2/Fe_3O_4 nanocomposite for MRI/PAI with image-guided photothermal therapy.[136] The T_2-weighted MRI accompanied with MT presented enhanced contrast after 24 h post injection. Subsequently, the same MT strategy was applied in PAI, enhanced contrast was observed after 0.5 and 6 h post injections. This example indicated the role of MT in multimodal bioimaging. Further to the composite structure of MoS_2 with Fe_3O_4, Liu et al. immobilized ^{64}Cu with MoS_2 and Fe_3O_4 via Cu-S adsorption to form a multifunctional platform for CT/PET/PAI (**Figure 6**(a)).[137] The PEGylation of the composite was tested in water, saline and glutathione prior to *in-vivo* multimodal bioimaging, it was found that double PEGylation (dPEG) exhibited the best stability in ionic condition. Figure 6(b) presents the time-dependent PET scans of the 4T1 tumor of mice as shown in Figure 6(e) suggested the effective passive targeting function of the composite after 3 h post injection. The PA images taken after intravenous injection of the composite (Figure 6(c)) indicated the even distribution of the composite around the tumor site. Moreover, the T_2 contrast of MRI in Figure 6(d) demonstrated substantial darkening of tumor site (red circle) and the liver due to accumulation of the composite after 24 h post injection. This also provided the fact about the uptake of the composite via the liver (blue arrow). Very recently, Lin and co-workers presented the use of MoS_2@Fe_3O_4-ICG/Pt(IV) nanoflowers for multimodal bioimaging and phototherapies.[138] The composite was prepared by a simple one-step hydrothermal method but it integrated three imaging modes and three therapeutic modes by singly 808 nm excitation. In addition to the MRI and PAI modes, the infrared thermal imaging can monitor the photothermal effect on the tumor in a real time manner. The hyper-integration and simple preparation provided an ideal platform for future theranostic applications. Aside from TMDs, graphene oxide (GO) and their composites played important role in the multimodal bioimaging application.[139,140] Liu and co-workers anchored SPIONs on reduced GO nanosheets for photothermal therapy and trimodal FI/PAI/MRI *in-vivo*.[141] The thorough surveys on the bioimaging ability,

biodistribution and toxicity provided grounds for future developments of using GOs-based composites for theranostic applications. In another report, Yang et al fabricated GO-conjugates to form an image-guided drug delivery platform for metastatic breast cancer.[142] The composite was labelled with the organic fluorophore fluorescein isothiocyanate and ^{64}Cu for FI/PET. Moreover, monoclonal antibody was used as the targeting agent to deliver the DOX to the cancer site. The composite showed superior drug delivery performance compared to GO. It is the fact that the QD counterparts of 2D TMDs were subject to strong quantum confinement due to the decreased dimension, which thus resulted in their unique energy band structures for multicolor emissions.[143,144] Recent reports indicated the 2D QDs only presented single FI modality, it is still worthwhile to examine their potential ability for future multimodality applications. Lin et al. fabricated the green luminescent BN QDs for cellular bioimaging.[145] In spite of their small size, the QDs could not reach the nuclei as revealed from the stained image. Xue et al. recently fabricated a new class of 2D early transition metal carbide Ti_3C_2 QDs by facile hydrothermal method and the crystalline size was simply tuned by the reaction temperature.[146] Interestingly, the QDs prepared at 150 °C showed acute toxicity while those at 100 and 120 °C showed very low toxicity. Encouraged by the low toxicity, the QDs were incubated with RAW264.7 cells for FI. The cells emitted blue, green and red emissions owing to the efficient uptake of the QDs via endocytosis. However, the QDs were still not able to penetrate the nuclei.

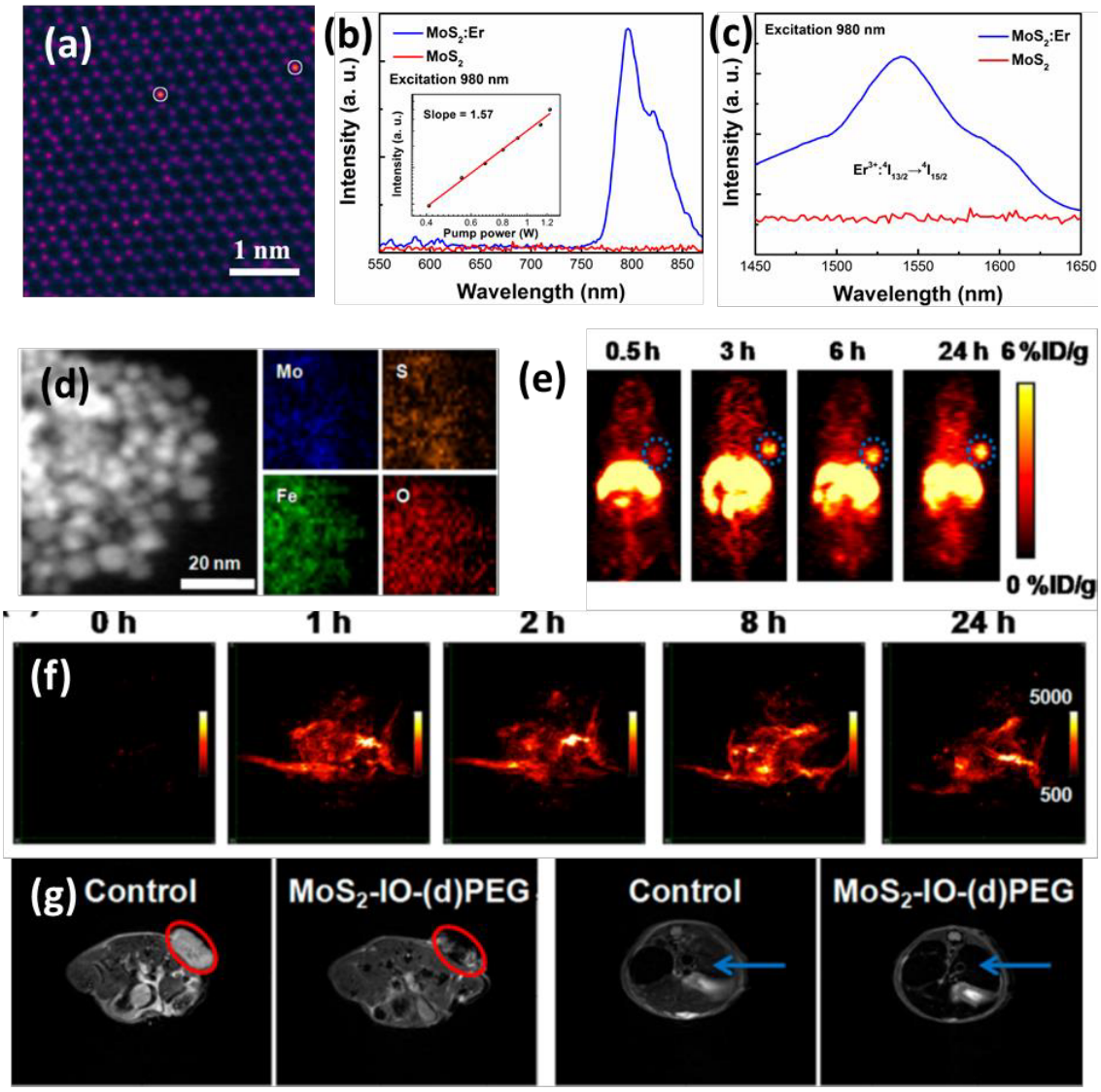

Figure 6. (a) STEM image of the Er-doped MoS_2 material, the Er atom was highlighted by circle. 980 nm laser excited NIR-NIR (b) UCL and (c) DSL emission spectra of the Er-doped MoS_2.[134] (d) STEM image and the corresponding elemental map analysis of elements in the ^{64}Cu-MoS_2-Fe_3O_4 composite. (e) PET scans and (f) PAI of the 4T1 tumor-bearing mice at different time post injection of the composite. (g) T_2-weighted MRI of the control and experimental groups with composite injection. The red circles indicate the tumor site while the blue arrows indicate the liver.[137]

4. Conclusions and perspectives

A wide spectrum of nanomaterials with different unique structures had been prepared by state-of-the art physical or chemical methods. Alongside with suitable surface functional groups and targeting moieties, they were able to perform multimodal bioimaging with outstanding contrast. The in-depth biodistribution studies can even support the clearance and retention of the nanomaterials at the region of interest. To date, numerous multimodal nanoprobes have been extensively reported and examined for bioimaging, but they were still limited by some factors. Au nanostructures are sensitive to pH and ionic strength of media; they may exhibit irreversible aggregation in the presence of inappropriate buffers or surface passivation.[147] Most of the nanoprobes can be purified by using solvents with centrifugations, the purification of functionalized and as-synthesized CQDs is relatively laborious because gel columns, dialysis or membrane filtering are needed for the extraction prior to bioimaging applications.[148-150] Ln^{3+} ions-doped UCNPs offer excellent physiochemical and optical properties that emerge as a competitive choice as nanoprobe, but the quantum yield (~5 %)[151] remains comparatively low to CQDs (~75 %).[152] The size distribution of NBs is large, usually at the range of several hundred nanometers.[153,154] The large distributions might affect the *in-vivo* bioimaging performance as the larger particles cannot enter small structures of targeted sites. Among the reviewed nanomaterials, 2D materials and their derivatives are a relatively new class of nanomaterials in bioimaging, hence their long term toxicity, immune response and clearance remain unclear.

The surveys on the long-term cytotoxicity of the nanomaterials and evaluations of their feasibility for future clinical diagnosis and medical imaging would be one of the future directions. The toxicity of nanomaterials stemmed from sizes, shapes, surface coatings, charges and release of chemical constituents. Some nanomaterials may even generate radicals under redox conditions that contribute to acute toxicity.[155,156] The toxicity of nanomaterials can be studied by different approaches, including behavior observation, body weight

measurement, histology analysis and hematology analysis in animal models[157] or cell viability, apoptosis, DNA damage and organ functions in cells lines.[156,158] Moreover, new methods were explored to increase the performance of toxicity analysis. Puzyn et al. presented the nano-quantitative structure activity relationship to predict the toxicity of metal oxides in bacteria[159] while Kandasamy et al. measured the toxicity of nanomaterials in cells by using the electric cell-substrate impedance sensing.[160] Despite the effort, the toxicity studies are constrained by the broad family of nanomaterials because of the vast combinations of elements. Therefore, it is difficult to generalize the toxicity of nanomaterials. The studies also cannot account for uncertainties for long term toxicity. Although computational algorithms had been developed to predict toxicity, expensive animal tests are still necessary to support the simulated results. In addition, it is also desirable to perform pre-clinical studies of novel nanomaterials for multimodal bioimaging. Such studies may contribute to the database of nanoprobes for future safety assessments. Detappe et al. presented their study on the dual modal MRI/CT image-guided radiation therapy.[161] They had mimic the existing clinical workflows for therapeutic agents. The flow of this study may be a useful reference for future image-guided therapy studies.

Apart from in-depth studies of the nanoprobes, the search for new, biocompatible and dischargeable nanoprobes should be continued with the stringent assessment on contrast ability and toxicity. It was demonstrated that the doping of Ln^{3+} ions into 2D materials can support luminescent bioimaging with high penetration. It is believed that this superior optical feature can be combined with the recently emerged 2D QDs for multimodal bioimaging, for instance BP QDs were able to provide PA contrast.[162] Recent works showed that the optical properties of new semiconductor QDs, such as Ag_2S[163] and PbS,[164] were tailored to emit light at NIR II window. They also demonstrated multimodal bioimaging by forming hybrid structures. In addition, the combination of NIR emissive Ln^{3+}-doped UCNPs with AuNRs had shown the subtissue localization at NIR II window and thermal monitoring ability by using

chicken breast tissue.[165] These reports indicated that imaging at NIR II window might be a future trend for FI. On the other hand, new bioimaging concepts might be introduced into the existing multimodal bioimaging systems. The dual-core mesoporous nanoparticles were able to control the temperature increment at nanoenvironment by using the hyperthermia effect of SPIONs.[166] The green UCL of Er^{3+} ions were used to monitor the localized temperature. Such effect might be potentially applied in biomedical imaging application. The concept of persistent luminescence bioimaging is helpful for long-term tracking and imaging, which would be an attractive research trend. Recent studies demonstrated rechargeable bioimaging by using NIR laser[167] and X-ray[168]; in particular the X-ray imaging can be synergistically cooperated with optical imaging for long-term monitoring. More advanced multimodal bioimaging systems can be developed based on these findings.

Acknowledgements

The research was financially supported by Innovation and Technology Support Programme (Project No. ITS/057/15) and Research Grants Council of Hong Kong (GRF No. PolyU 153281/16P).

Received: ((will be filled in by the editorial staff))
Revised: ((will be filled in by the editorial staff))
Published online: ((will be filled in by the editorial staff))

References

[1] S. L.Jacques, *Phys. Med. Biol.* **2013**, *58*, R37.

[2] ICRU, *Tissue Substitutes in Radiation Dosimetry and Measurement (Report 44)*, The International Commission On Radiation Units And Measurements, Bethesda, MD, **1989**.

[3] E. M.Strohm, M. C.Kolios, *Cytom. Part A* **2015**, *87*, 741.

[4] A.VNaumova, M.Modo, A.Moore, C. E.Murry, J. A.Frank, *Nat. Biotechnol.* **2014**, *32*, 804.

[5] D. P.Cormode, P. C.Naha, Z. A.Fayad, *Contrast Media Mol. Imaging* **2014**, *9*, 37.

[6] Y.Sun, M.Yu, S.Liang, Y.Zhang, C.Li, T.Mou, W.Yang, X.Zhang, B.Li, C.Huang, F.Li, *Biomaterials* **2011**, *32*, 2999.

[7] J.Ramalho, R. C.Semelka, M.Ramalho, R. H.Nunes, M.AlObaidy, M.Castillo, *Am. J. Neuroradiol.* **2016**, *37*, 1192.

[8] M.Bruchez Jr., M.Moronne, P.Gin, S.Weiss, A. P.Alivisatos, *Science (80-.).* **1998**, *281*, 2013.

[9] A. L.Efros, D. J.Nesbitt, *Nat. Nanotechnol.* **2016**, *11*, 661.

[10] A. M.Derfus, W. C. W.Chan, S. N.Bhatia, *Nano Lett.* **2004**, *4*, 11.

[11] R. R.Anderson, J. A.Parrish, *J. Invest. Dermatol.* **1981**, *77*, 13.

[12] C. R.Anderson, X.Hu, H.Zhang, J.Tlaxca, A.-E.Declèves, R.Houghtaling, K.Sharma, M.Lawrence, K. W.Ferrara, J. J.Rychak, *Invest. Radiol.* **2011**, *46*, 215.

[13] C. F.Caskey, S. M.Stieger, S.Qin, P. aDayton, K. W.Ferrara, *J. Acoust. Soc. Am.* **2007**, *122*, 1191.

[14] M. J. K.Blomley, J. C.Cooke, E. C.Unger, M. J.Monaghan, D. O.Cosgrove, *Bmj* **2001**, *322*, 1222.

[15] E.Huynh, J. F.Lovell, B. L.Helfield, M.Jeon, C.Kim, D. E.Goertz, B. C.Wilson,

G.Zheng, *J. Am. Chem. Soc.* **2012**, *134*, 16464.

[16] E.Huynh, C. S.Jin, B. C.Wilson, G.Zheng, *Bioconjug. Chem.* **2014**, *25*, 796.

[17] M.Meng, J.Gao, C.Wu, X.Zhou, X.Zang, X.Lin, H.Liu, C.Wang, H.Su, K.Liu, Y.Wang, X.Xue, J.Wu, *Tumor Biol.* **2016**, *37*, 8673.

[18] J.Rieffel, U.Chitgupi, J. F.Lovell, *Small* **2015**, *11*, 4445.

[19] B. R.Smith, S. S.Gambhir, *Chem. Rev.* **2017**, *117*, 901.

[20] X.Li, J.Kim, J.Yoon, X.Chen, *Adv. Mater.* **2017**, *29*, 1606857.

[21] J.Wang, Q.Ma, Y.Wang, H.Shen, Q.Yuan, *Nanoscale* **2017**, *9*, 6204.

[22] S. Y.Lim, W.Shen, Z.Gao, *Chem. Soc. Rev.* **2015**, *44*, 362.

[23] J.Liu, L.Gong, Y.Wang, *Biomater. Sci.* **2017**, *5*, 1393.

[24] J.-E.Park, M.Kim, J.-H.Hwang, J.-M.Nam, *Small Methods* **2017**, *1*, 1600032.

[25] S.Chen, H.Wang, Y.Hong, B. Z.Tang, *Mater. Horiz.* **2016**, *3*, 283.

[26] Y.Cui, Y.Yue, G.Qian, B.Chen, *Chem. Rev.* **2012**, *112*, 1126.

[27] V.Kapoor, B. M.McCook, F. S.Torok, *RadioGraphics* **2004**, *24*, 523.

[28] R.Madru, P.Svenmarker, C.Ingvar, F.Ståhlberg, S.-A.Engels, L.Knutsson, S.-E.Strand, *Diagnostics* **2014**, *4*, 13.

[29] R.Weissleder, *Nat. Biotechnol.* **2001**, *19*, 316.

[30] G.Hong, J. C.Lee, J. T.Robinson, U.Raaz, L.Xie, N. F.Huang, J. P.Cooke, H.Dai, *Nat. Med.* **2012**, *18*, 1841.

[31] G.Hong, S.Diao, J.Chang, A. L.Antaris, C.Chen, B.Zhang, S.Zhao, D. N.Atochin, P. L.Huang, K. I.Andreasson, C. J.Kuo, H.Dai, *Nat. Photonics* **2014**, *8*, 723.

[32] S.Zeng, M.-K.Tsang, C.-F.Chan, K.-L.Wong, J.Hao, *Biomaterials* **2012**, *33*, 9232.

[33] C.Chen, J.Liu, Y.Chen, C.Li, X.Liu, H.Huang, C.Liang, Y.Lou, Z.Shi, S.Feng, *ACS Appl. Mater. Interfaces* **2017**, *9*, 5748.

[34] Z.Yi, X.Li, Z.Xue, X.Liang, W.Lu, H.Peng, H.Liu, S.Zeng, J.Hao, *Adv. Funct. Mater.* **2015**, *25*, 7119.

[35] M.Fernández-Suárez, A. Y.Ting, *Nat. Rev. Mol. Cell Biol.* **2008**, *9*, 929.

[36] T.Chailangkarn, C. A.Trujillo, B. C.Freitas, B.Hrvoj-Mihic, R. H.Herai, D. X.Yu, T. T.Brown, M. C.Marchetto, C.Bardy, L.McHenry, L.Stefanacci, A.Järvinen, Y. M.Searcy, M.DeWitt, W.Wong, P.Lai, M. C.Ard, K. L.Hanson, S.Romero, B.Jacobs, A. M.Dale, L.Dai, J. R.Korenberg, F. H.Gage, U.Bellugi, E.Halgren, K.Semendeferi, A. R.Muotri, *Nature* **2016**, *536*, 338.

[37] L.Cheng, J.Liu, X.Gu, H.Gong, X.Shi, T.Liu, C.Wang, X.Wang, G.Liu, H.Xing, W.Bu, B.Sun, Z.Liu, *Adv. Mater.* **2014**, *26*, 1886.

[38] J.Hedhli, A.Czerwinski, M. R.Schuelke, A.Ploska, L.LaHood, P.Czaplewska, S. B.Mamer, I. T.Dobrucki, P.Sowinski, L.Kalinowski, P. I.Imoukhuede, L. W.Dobrucki, *Sci. Rep.* **2017**, *7*, 3185.

[39] S. L.Pimlott, A.Sutherland, *Chem. Soc. Rev.* **2011**, *40*, 149.

[40] Y.Zhao, B.Pang, H.Luehmann, L.Detering, X.Yang, D.Sultan, S.Harpstrite, V.Sharma, C. S.Cutler, Y.Xia, Y.Liu, *Adv. Healthc. Mater.* **2016**, *5*, 928.

[41] S.Mallidi, K.Watanabe, D.Timerman, D.Schoenfeld, T.Hasan, *Theranostics* **2015**, *5*, 289.

[42] R. J.Paproski, A.Forbrich, E.Huynh, J.Chen, J. D.Lewis, G.Zheng, R. J.Zemp, *Small* **2016**, *12*, 371.

[43] L.V.Wang, S.Hu, *Science (80-.).* **2012**, *335*, 1458.

[44] A.Sedlmeier, H. H.Gorris, *Chem. Soc. Rev.* **2015**, *44*, 1526.

[45] Y.Chen, Y.Xianyu, X.Jiang, *Acc. Chem. Res.* **2017**, *50*, 310.

[46] B.Liu, J.Liu, *Nano Res.* **2017**, *10*, 1125.

[47] G.Bai, M.-K.Tsang, J.Hao, *Adv. Funct. Mater.* **2016**, *26*, 6330.

[48] W. W.Ye, M.-K.Tsang, X.Liu, M.Yang, J.Hao, *Small* **2014**, *10*, 2390.

[49] X.Ning, C.Peng, E. S.Li, J.Xu, R. D.Vinluan, M.Yu, J.Zheng, *APL Mater.* **2017**, *5*, 53406.

[50] M.Yu, J.Liu, X.Ning, J.Zheng, *Angew. Chemie - Int. Ed.* **2015**, *54*, 15434.

[51] M.Yu, J.Zhou, B.Du, X.Ning, C.Authement, L.Gandee, P.Kapur, J. T.Hsieh, J.Zheng, *Angew. Chemie - Int. Ed.* **2016**, *55*, 2787.

[52] Y.Chong, Y.Ma, H.Shen, X.Tu, X.Zhou, J.Xu, J.Dai, S.Fan, Z.Zhang, *Biomaterials* **2014**, *35*, 5041.

[53] Z.Khatun, K. M.Huh, S. Y.Park, D. Y.Lee, K. J.Cho, Y.Lee, *ACS Nano* **2013**, *7*, 6858.

[54] K.Yang, H.Gong, X.Shi, J.Wan, Y.Zhang, Z.Liu, *Biomaterials* **2013**, *34*, 2787.

[55] A.Cayuela, M. L.Soriano, C.Carrillo-Carrión, M.Valcárcel, *Chem. Commun.* **2016**, *52*, 1311.

[56] L.Tang, R.Ji, X.Cao, J.Lin, H.Jiang, X.Li, K. S.Teng, C. M.Luk, S.Zeng, J.Hao, S. P.Lau, *ACS Nano* **2012**, *6*, 5102.

[57] B. M.Hutchins, T. T.Morgan, M. G.Ucak-Astarlioglu, M.Elizabeth Williams, *J. Chem. Educ.* **2007**, *84*, 1301.

[58] M. K. G.Jayakumar, N. M.Idris, K.Huang, Y.Zhang, *Nanoscale* **2014**, *6*, 8441.

[59] F.Wang, R.Deng, J.Wang, Q.Wang, Y.Han, H.Zhu, X.Chen, X.Liu, *Nat. Mater.* **2011**, *10*, 968.

[60] B.Liu, C.Li, P.Yang, Z.Hou, J.Lin, *Adv. Mater.* **2017**, *29*, 1605434.

[61] F.Wang, D.Banerjee, Y.Liu, X.Chen, X.Liu, *Analyst* **2010**, *135*, 1839.

[62] G.Tian, Z.Gu, L.Zhou, W.Yin, X.Liu, L.Yan, S.Jin, W.Ren, G.Xing, S.Li, Y.Zhao, *Adv. Mater.* **2012**, *24*, 1226.

[63] M.-K.Tsang, W.Ye, G.Wang, J.Li, M.Yang, J.Hao, *ACS Nano* **2016**, *10*, 598.

[64] C.Chen, C.Li, Z.Shi, *Adv. Sci.* **2016**, *3*, 1600029.

[65] H.Liu, W.Lu, H.Wang, L.Rao, Z.Yi, S.Zeng, J.Hao, *Nanoscale* **2013**, *5*, 6023.

[66] Z.Yi, S.Zeng, W.Lu, H.Wang, L.Rao, H.Liu, J.Hao, *ACS Appl. Mater. Interfaces* **2014**, *6*, 3839.

[67] M.Alheshibri, J.Qian, M.Jehannin, V. S. J.Craig, *Langmuir* **2016**, *32*, 11086.

[68] S.Yuan, Z.Yang, C.Xie, F.Yan, J.Dai, S. P.Lau, H. L. W.Chan, J.Hao, *Adv. Mater.* **2016**, *28*, 10048.

[69] W.Jie, X.Chen, D.Li, L.Xie, Y. Y.Hui, S. P.Lau, X.Cui, J.Hao, *Angew. Chemie - Int. Ed.* **2015**, *54*, 1185.

[70] W.Jie, Z.Yang, F.Zhang, G.Bai, C. W.Leung, J.Hao, *ACS Nano* **2017**, *11*, 6950.

[71] Z.Yang, W.Jie, C. H.Mak, S.Lin, H.Lin, X.Yang, F.Yan, S. P.Lau, J.Hao, *ACS Nano* **2017**, *11*, 4225.

[72] T.Wu, H.Zhang, *Angew. Chemie - Int. Ed.* **2015**, *54*, 4432.

[73] K.Yang, S.Zhang, G.Zhang, X.Sun, S. T.Lee, Z.Liu, *Nano Lett.* **2010**, *10*, 3318.

[74] C.Chung, Y.Kim, D.Shin, S.Ryoo, B. H. E. E.Hong, D.Min, *Acc. Chem. Res.* **2013**, *46*, 2211.

[75] Y.Chen, C.Tan, H.Zhang, L.Wang, *Chem. Soc. Rev.* **2015**, *44*, 2681.

[76] X.Zhang, X.Xie, H.Wang, J.Zhang, B.Pan, Y.Xie, *J. Am. Chem. Soc.* **2013**, *135*, 18.

[77] Z.Lei, W.Zhu, S.Xu, J.Ding, J.Wan, P.Wu, *ACS Appl. Mater. Interfaces* **2016**, *8*, 20900.

[78] L.Chen, X.Zhou, W.Nie, W.Feng, Q.Zhang, W.Wang, Y.Zhang, Z.Chen, P.Huang, C.He, *ACS Appl. Mater. Interfaces* **2017**, *9*, 17786.

[79] W. Z.Teo, E. L. K.Chng, Z.Sofer, M.Pumera, *Chem. - A Eur. J.* **2014**, *20*, 9627.

[80] D. H.Xie, D. K.Ji, Y.Zhang, J.Cao, H.Zheng, L.Liu, Y.Zang, J.Li, G. R.Chen, T. D.James, X. P.He, *Chem. Commun.* **2016**, *52*, 9418.

[81] J.Mao, P.Chen, J.Liang, R.Guo, L. T.Yan, *ACS Nano* **2016**, *10*, 1493.

[82] X.Wang, G.Sun, N.Li, P.Chen, *Chem. Soc. Rev.* **2016**, *45*, 2239.

[83] Y.You, Q.Song, L.Wang, C.Niu, N.Na, J.Ouyang, *Nanoscale* **2016**, *8*, 18150.

[84] X.Li, L.Xing, K.Zheng, P.Wei, L.Du, M.Shen, X.Shi, *ACS Appl. Mater. Interfaces* **2017**, *9*, 5817.

[85] X.-Q.Wang, F.Gao, X.-Z.Zhang, *Angew. Chemie Int. Ed.* **2017**, 1.

[86] Y.Jin, *Acc. Chem. Res.* **2014**, *47*, 138.

[87] K.Cheng, S.Kothapalli, H.Liu, A. L.Koh, J.VJokerst, H.Jiang, M.Yang, J.Li, J.Levi, J. C.Wu, S. S.Gambhir, Z.Cheng, *J. Am. Chem. Soc.* **2014**, *136*, 3560.

[88] L.Huang, L.Ao, D.Hu, W.Wang, Z.Sheng, W.Su, *Chem. Mater.* **2016**, *28*, 5896.

[89] M.Li, L.Li, C.Zhan, D. S.Kohane, *Theranostics* **2016**, *6*, 2306.

[90] L.Han, J. M.Xia, X.Hai, Y.Shu, X. W.Chen, J. H.Wang, *ACS Appl. Mater. Interfaces* **2017**, *9*, 6941.

[91] P.Crespo, R.Litrán, T. C.Rojas, M.Multigner, J. M.DeLa Fuente, J. C.Sánchez-López, M. A.García, A.Hernando, S.Penadés, A.Fernández, *Phys. Rev. Lett.* **2004**, *93*, 87204.

[92] C.Zhao, T.Du, F. urRehman, L.Lai, X.Liu, X.Jiang, X.Li, Y.Chen, H.Zhang, Y.Sun, S.Luo, H.Jiang, M.Selke, X.Wang, *Small* **2016**, *12*, 6255.

[93] M.Hembury, C.Chiappini, S.Bertazzo, T. L.Kalber, G. L.Drisko, O.Ogunlade, S.Walker-Samuel, K. S.Krishna, C.Jumeaux, P.Beard, C. S. S. R.Kumar, A. E.Porter, M. F.Lythgoe, C.Boissière, C.Sanchez, M. M.Stevens, *Proc. Natl. Acad. Sci. U. S. A.* **2015**, *112*, 1959.

[94] C.Lee, W.Kwon, S.Beack, D.Lee, Y.Park, H.Kim, S. K.Hahn, S. W.Rhee, C.Kim, *Theranostics* **2016**, *6*, 2196.

[95] L.Wu, X.Cai, K.Nelson, W.Xing, J.Xia, R.Zhang, A. J.Stacy, M.Luderer, G. M.Lanza, L.V.Wang, B.Shen, D.Pan, *Nano Res.* **2013**, *6*, 312.

[96] S.Zanganeh, H.Li, P. D.Kumavor, U.Alqasemi, A.Aguirre, I.Mohammad, C.Stanford, M. B.Smith, Q.Zhu, *J. Biomed. Opt.* **2013**, *18*, 96006.

[97] A. D.LaZerda, Z.Liu, S.Bodapati, R.Teed, S.Vaithilingam, B. T.Khuri-Yakub, X.Chen, H.Dai, S. S.Gambhir, *Nano Lett.* **2010**, *10*, 2168.

[98] A.DeLa Zerda, C.Zavaleta, S.Keren, S.Vaithilingam, S.Bodapati, Z.Liu, J.Levi, B. R.Smith, T.-J.Ma, O.Oralkan, Z.Cheng, X.Chen, H.Dai, B. T.Khuri-Yakub, S. S.Gambhir, *Nat. Nanotechnol.* **2008**, *3*, 557.

[99] L.Xie, G.Wang, H.Zhou, F.Zhang, Z.Guo, C.Liu, X.Zhang, L.Zhu, *Biomaterials* **2016**,

103, 219.

[100] H.Chen, L.Wang, H.Fu, Z.Wang, Y.Xie, Z.Zhang, Y.Tang, *J. Mater. Chem. B* **2016**, *4*, 7472.

[101] F.Du, M.Zhang, A.Gong, Y.Tan, J.Miao, Y.Gong, S.Zou, L.Zhang, L.Zhang, C.Wu, M.Sun, H.Ju, C.Wu, S.Zou, *Biomaterials* **2017**, *121*, 109.

[102] Y.Pan, J.Yang, Y.Fang, J.Zheng, R.Song, C.Yi, *J. Mater. Chem. B* **2017**, *5*, 92.

[103] S.-T.Yang, L.Cao, P. G.Luo, F.Lu, X.Wang, H.Wang, M. J.Meziani, Y.Liu, G.Qi, Y.-P.Sun, *J. Am. Chem. Soc.* **2009**, *131*, 11308.

[104] M.Zheng, S.Ruan, S.Liu, T.Sun, D.Qu, H.Zhao, Z.Xie, H.Gao, X.Jing, Z.Sun, *ACS Nano* **2015**, *9*, 11455.

[105] X.Su, C.Chan, J.Shi, M. K.Tsang, Y.Pan, C.Cheng, O.Gerile, M.Yang, *Biosens. Bioelectron.* **2017**, *92*, 489.

[106] X.Liu, H.Jiang, J.Ye, C.Zhao, S.Gao, C.Wu, C.Li, J.Li, X.Wang, *Adv. Funct. Mater.* **2016**, *26*, 8694.

[107] Y. Y.Yao, G.Gedda, W. M.Girma, C. L.Yen, Y. C.Ling, J. Y.Chang, *ACS Appl. Mater. Interfaces* **2017**, *9*, 13887.

[108] J.Ge, Q.Jia, W.Liu, L.Guo, Q.Liu, M.Lan, H.Zhang, X.Meng, P.Wang, *Adv. Mater.* **2015**, *27*, 4169.

[109] S.Han, A.Samanta, X.Xie, L.Huang, J.Peng, S. J.Park, D. B. L.Teh, Y.Choi, Y. T.Chang, A. H.All, Y.Yang, B.Xing, X.Liu, *Adv. Mater.* **2017**, *29*, 1700244.

[110] H.Chen, B.Qi, T.Moore, D. C.Colvin, T.Crawford, J. C.Gore, F.Alexis, O. T.Mefford, J. N.Anker, *Small* **2014**, *10*, 160.

[111] X.Zhang, Z.Zhao, X.Zhang, D. B.Cordes, B.Weeks, B.Qiu, K.Madanan, D.Sardar, J.Chaudhuri, *Nano Res.* **2015**, *8*, 636.

[112] C.Liu, Z.Gao, J.Zeng, Y.Hou, F.Fang, Y.Li, R.Qiao, L.Shen, *ACS Nano* **2013**, *7*, 7227.

[113] S.Zeng, M.-K.Tsang, C.-F.Chan, K.-L.Wong, B.Fei, J.Hao, *Nanoscale* **2012**, *4*, 5118.

[114] J.Wang, H.Zhang, D.Ni, W.Fan, J.Qu, Y.Liu, Y.Jin, Z.Cui, T.Xu, Y.Wu, W.Bu, Z.Yao, *Small* **2016**, *12*, 3591.

[115] Y.-F.Wang, G.-Y.Liu, L.-D.Sun, J.-W.Xiao, J.-C.Zhou, C.-H.Yan, *ACS Nano* **2013**, *7*, 7200.

[116] Y.Li, J.Tang, D. X.Pan, L. D.Sun, C.Chen, Y.Liu, Y. F.Wang, S.Shi, C. H.Yan, *ACS Nano* **2016**, *10*, 2766.

[117] Y.Li, J.Tang, L.He, Y.Liu, Y.Liu, C.Chen, Z.Tang, *Adv. Mater.* **2015**, *27*, 4075.

[118] Y.Liu, N.Kang, J.Lv, Z.Zhou, Q.Zhao, L.Ma, Z.Chen, *Adv. Mater.* **2016**, *28*, 6411.

[119] J.Zhou, M.Yu, Y.Sun, X.Zhang, X.Zhu, Z.Wu, D.Wu, F.Li, *Biomaterials* **2011**, *32*, 1148.

[120] J.Peng, Y.Sun, L.Zhao, Y.Wu, W.Feng, Y.Gao, F.Li, *Biomaterials* **2013**, *34*, 9535.

[121] Y.Sun, X.Zhu, J.Peng, F.Li, *ACS Nano* **2013**, *7*, 11290.

[122] J.Rieffel, F.Chen, J.Kim, G.Chen, W.Shao, S.Shao, U.Chitgupi, R.Hernandez, S. A.Graves, R. J.Nickles, P. N.Prasad, C.Kim, W.Cai, J. F.Lovell, *Adv. Mater.* **2015**, *27*, 1785.

[123] M.Sun, L.Xu, W.Ma, X.Wu, H.Kuang, L.Wang, C.Xu, *Adv. Mater.* **2016**, *28*, 898.

[124] X.Fan, L.Wang, Y.Guo, H.Tong, L.Li, J.Ding, H.Huang, *Nanotechnology* **2013**, *24*, 325102.

[125] H.Yang, W.Cai, L.Xu, X.Lv, Y.Qiao, P.Li, H.Wu, Y.Yang, L.Zhang, Y.Duan, *Biomaterials* **2015**, *37*, 279.

[126] W.Song, Y.Luo, Y.Zhao, X.Liu, J.Zhao, J.Luo, Q.Zhang, H.Ran, Z.Wang, D.Guo, *Nanomedicine* **2017**, *12*, 991.

[127] M.-K.Tsang, G.Bai, J.Hao, *Chem. Soc. Rev.* **2015**, *44*, 1585.

[128] E. G.Kelley, J. N. L.Albert, M. O.Sullivan, T. H.Epps, *Chem. Soc. Rev.* **2013**, *42*, 7057.

[129] H. Y.Huang, S. H.Hu, S. Y.Hung, C. S.Chiang, H. L.Liu, T. L.Chiu, H. Y.Lai, Y. Y.Chen, S. Y.Chen, *J. Control. Release* **2013**, *172*, 118.

[130] Y.Liu, F.Yang, C.Yuan, M.Li, T.Wang, B.Chen, J.Jin, P.Zhao, J.Tong, S.Luo, N.Gu, *ACS Nano* **2017**, *11*, 1509.

[131] A.Hannah, G.Luke, K.Wilson, K.Homan, S.Emelianov, *ACS Nano* **2014**, *8*, 250.

[132] E.Huynh, B. Y. C.Leung, B. L.Helfield, M.Shakiba, J.-A.Gandier, C. S.Jin, E. R.Master, B. C.Wilson, D. E.Goertz, G.Zheng, *Nat. Nanotechnol.* **2015**, *10*, 325.

[133] S. Z.Butler, S. M.Hollen, L.Cao, Y.Cui, J. A.Gupta, H. R.Gutiérrez, T. F.Heinz, S. S.Hong, J.Huang, A. F.Ismach, E.Johnston-Halperin, M.Kuno, V.V.Plashnitsa, R. D.Robinson, R. S.Ruoff, S.Salahuddin, J.Shan, L.Shi, M. G.Spencer, M.Terrones, W.Windl, J. E.Goldberger, *ACS Nano* **2013**, *7*, 2898.

[134] G.Bai, S.Yuan, Y.Zhao, Z.Yang, S. Y.Choi, Y.Chai, S. F.Yu, S. P.Lau, J.Hao, *Adv. Mater.* **2016**, *28*, 7472.

[135] S.Wang, X.Li, Y.Chen, X.Cai, H.Yao, W.Gao, Y.Zheng, X.An, J.Shi, H.Chen, *Adv. Mater.* **2015**, *27*, 2775.

[136] J.Yu, W.Yin, X.Zheng, G.Tian, X.Zhang, T.Bao, X.Dong, Z.Wang, Z.Gu, X.Ma, Y.Zhao, *Theranostics* **2015**, *5*, 931.

[137] T.Liu, S.Shi, C.Liang, S.Shen, L.Cheng, C.Wang, X.Song, S.Goel, B.Todd E., C.Weibo, L.Zhuang, *ACS Nano* **2015**, 950.

[138] B.Liu, C.Li, G.Chen, B.Liu, X.Deng, Y.Wei, J.Xia, *Adv. Sci.* **2017**, *4*, 1600540.

[139] P.Rong, J.Wu, Z.Liu, X.Ma, L.Yu, K.Zhou, W.Zeng, W.Wang, *RSC Adv.* **2016**, *6*, 1894.

[140] H.Zhang, H.Wu, J.Wang, Y.Yang, D.Wu, Y.Zhang, Y.Zhang, Z.Zhou, S.Yang, *Biomaterials* **2015**, *42*, 66.

[141] K.Yang, L.Hu, X.Ma, S.Ye, L.Cheng, X.Shi, C.Li, Y.Li, Z.Liu, *Adv. Mater.* **2012**, *24*, 1868.

[142] D.Yang, L.Feng, C.Dougherty, D.Chen, Z.Liu, H.Hong, *J. Nucl. Med.* **2016**, *57*, 193.

[143] X.Bai, J.Wang, X.Mu, J.Yang, H.Liu, F.Xu, Y.Jing, L.Liu, X.Xue, H.Dai, Q.Liu, Y.

M.Sun, C.Liu, X. D.Zhang, *ACS Biomater. Sci. Eng.* **2017**, *3*, 460.

[144] S.Xu, D.Li, P.Wu, *Adv. Funct. Mater.* **2015**, *25*, 1127.

[145] L.Lin, Y.Xu, S.Zhang, I. M.Ross, A. C. M.Ong, D. A.Allwood, *Small* **2014**, *10*, 60.

[146] Q.Xue, H.Zhang, M.Zhu, Z.Pei, H.Li, Z.Wang, Y.Huang, Y.Huang, Q.Deng, J.Zhou, S.Du, Q.Huang, C.Zhi, *Adv. Mater.* **2017**, *29*, 1604847.

[147] X.Zhang, M. R.Servos, J.Liu, *J. Am. Chem. Soc.* **2012**, *134*, 7266.

[148] Y.Dong, N.Zhou, X.Lin, J.Lin, Y.Chi, G.Chen, *Chem. Mater.* **2010**, *22*, 5895.

[149] Y.Zhao, Y.Zhang, X.Liu, H.Kong, Y.Wang, G.Qin, P.Cao, X.Song, X.Yan, Q.Wang, H.Qu, *Sci. Rep.* **2017**, *7*, 4452.

[150] L.Cao, S. T.Yang, X.Wang, P. G.Luo, J. H.Liu, S.Sahu, Y.Liu, Y. P.Sun, *Theranostics* **2012**, *2*, 295.

[151] X.Wu, Y.Zhang, K.Takle, O.Bilsel, Z.Li, H.Lee, Z.Zhang, D.Li, W.Fan, C.Duan, E. M.Chan, C.Lois, Y.Xiang, G.Han, *ACS Nano* **2016**, *10*, 1060.

[152] F.Yuan, Z.Wang, X.Li, Y.Li, Z.Tan, L.Fan, S.Yang, *Adv. Mater.* **2017**, *29*, DOI 10.1002/adma.201604436.

[153] W.BinCai, H. L.Yang, J.Zhang, J. K.Yin, Y. L.Yang, L. J.Yuan, L.Zhang, Y. Y.Duan, *Sci. Rep.* **2015**, *5*, 13725.

[154] M.Zhang, J. R. T.Seddon, *Langmuir* **2016**, *32*, 11280.

[155] G.Lynn, C.Christine, Eds., *Implications of Nanotechnology for Environmental Health Research*, National Academies Press (US), **2005**.

[156] K. T.Butterworth, J. A.Coulter, S.Jain, J.Forker, S. J.McMahon, G.Schettino, K. M.Prise, F. J.Currell, D. G.Hirst, *Nanotechnology* **2010**, *21*, 295101.

[157] F.Zhang, *Photon Upconversion Nanomaterials*, Springer, Berlin Heidelberg, **2015**.

[158] L.Braydich-Stolle, S.Hussain, J. J.Schlager, M. C.Hofmann, *Toxicol. Sci.* **2005**, *88*, 412.

[159] T.Puzyn, B.Rasulev, A.Gajewicz, X.Hu, T. P.Dasari, A.Michalkova, H.-M.Hwang, A.Toropov, D.Leszczynska, J.Leszczynski, *Nat. Nanotechnol.* **2011**, *6*, 175.

[160] K.Kandasamy, C. S.Choi, S.Kim, *Nanotechnology* **2010**, *21*, 375501.

[161] A.Detappe, E.Thomas, M. W.Tibbitt, S.Kunjachan, O.Zavidij, N.Parnandi, E.Reznichenko, F.Lux, O.Tillement, R.Berbeco, *Nano Lett.* **2017**, *17*, 1733.

[162] C.Sun, L.Wen, J.Zeng, Y.Wang, Q.Sun, L.Deng, C.Zhao, Z.Li, *Biomaterials* **2016**, *91*, 81.

[163] C.Wu, Y.Zhang, Z.Li, C.Li, Q.Wang, *Nanoscale* **2016**, 12531.

[164] D. H.Ortgies, L.DeLa Cueva, B.DelRosal, F.Sanz-Rodríguez, N.Fernández, M. C.Iglesias-De La Cruz, G.Salas, D.Cabrera, F. J.Teran, D.Jaque, E.Martín Rodríguez, *ACS Appl. Mater. Interfaces* **2016**, *8*, 1406.

[165] U.Rocha, J.Hu, E. M.Rodríguez, A. S.Vanetsev, M.Rähn, V.Sammelselg, Y.V.Orlovskii, J. G.Solé, D.Jaque, D. H.Ortgies, *Small* **2016**, *12*, 5394.

[166] J.Dong, J. I.Zink, *ACS Nano* **2014**, *8*, 5199.

[167] S.Zeng, Z.Xue, X.Li, Y.Li, Y.Jiang, G.Ren, H.Liu, J.Hao, *Nanoscale* **2017**, *9*, 7276.

[168] Z.Xue, X.Li, Y.Li, M.Jiang, H.Liu, S.Zeng, J.Hao, *ACS Appl. Mater. Interfaces* **2017**, *9*, 22132.